

Physics-based parametrization of the surface impedance for radio frequency sheaths

J. R. Myra

Lodestar Research Corporation, Boulder, CO, USA

April 2017

DOE-ER/54823-19; DOE-ER/54392-86

LRC-17-170

LODESTAR RESEARCH CORPORATION

*2400 Central Avenue
Boulder, Colorado 80301*

Physics-based parametrization of the surface impedance for radio frequency sheaths

J. R. Myra

Lodestar Research Corporation, 2400 Central Avenue, Boulder, Colorado 80301

Abstract

The properties of sheaths near conducting surfaces are studied for the case where both magnetized plasma and intense radio frequency (rf) waves coexist. The work is motivated primarily by the need to understand, predict and control ion cyclotron range of frequency (ICRF) interactions with tokamak scrape-off layer plasmas, and is expected to be useful in modeling rf sheath interactions in global ICRF codes. Employing a previously developed model for oblique angle magnetized rf sheaths [J. R. Myra and D. A. D'Ippolito, *Phys. Plasmas* **22**, 062507 (2015)], an investigation of the four-dimensional parameter space governing these sheath is carried out. By combining numerical and analytical results, a parametrization of the surface impedance and voltage rectification for rf sheaths in the entire four-dimensional space is obtained.

Keywords: radio-frequency, sheath, impedance, rectification, magnetized, ICRF, tokamak

I. Introduction

Ion cyclotron range of frequency (ICRF) waves are expected to play an increasingly important role as tokamak research progresses towards the reactor regime. While ICRF waves have been successfully used in many present day experiments for heating and current drive, there are some regimes in which excessive unwanted interactions with the antenna and/or boundary plasma are observed. It is important to understand, predict and control these interactions.

It is believed that rf sheaths, which form on material surfaces, are responsible for enhanced impurity sputtering and self-sputtering, parasitic power dissipation, hot spots, and reduced heating efficiency of the core plasma. Learning how to model and quantitatively predict the magnitude of these rf sheath interactions for a given set of conditions is an important challenge facing the theory and numerical simulation communities. Reviews of experimental and theoretical work on ICRF edge and wall interactions are given in Refs. 1-2 and a short overview of the sheath physics can be found in Ref. 3. More recently, these issues have been the subject of experimental investigations on many tokamaks,⁴⁻¹¹ and linear test stands^{12,13} and the topic given rise to a number of dedicated modeling efforts.¹⁴⁻²¹

A promising technique for modeling sheath interactions is the use of an rf sheath boundary condition (BC)²² at the sheath-plasma interface. This approach prevents having to directly model disparate space scales in the same code: the tiny Debye-scale sheath and global rf wave propagation. The earliest forms of a sheath BC²²⁻²⁴ invoked a capacitive limit²⁵ in which the Debye-scale sheath, nearly devoid of current carrying electrons, was treated as a thin vacuum layer. This approximation often suffices in the high frequency limit $\omega > \omega_{pi}$, where ω is the rf wave frequency and ω_{pi} is the ion plasma frequency. In that limit the rf ion response is small (the so called “immobile ion” regime) and the main current across the sheath is the displacement current. More recently,²⁶ the capacitive sheath BC was generalized to a sheath impedance BC with both real and imaginary parts. This complex sheath impedance additionally describes the effective sheath resistance at rf frequencies, important for modeling localized rf power deposition. In that work,²⁶ it was shown that the sheath impedance depends on four dimensionless input parameters: the degree of sheath magnetization, the magnetic field angle with the surface, a normalized rf field strength and the degree of ion mobility set by the wave frequency. A nonlinear Debye-scale rf model was developed to calculate the effective sheath impedance at the rf frequency, and results were presented for selected parameters and scans. Other work generalizing the capacitive rf sheath model has been carried out in the plasma processing literature,²⁷ although this field has almost always considered perpendicular (equivalently unmagnetized) sheaths.

For practical implementation of a sheath BC in global codes, a *robust* subroutine must be able to return the sheath impedance quickly and accurately, ideally for *any* set of input parameters. With present day emphasis on massively parallel large scale computations, where a very large number of BC subroutine calls may be made in a computationally expensive simulation, the importance of robustness cannot be overemphasized. While in principle the impedance can be calculated using the methods of Ref. 26 for almost any set of input parameters, in practice some tuning of numerical parameters (such as time and space resolution and numerical system size) is required for convergence and acceptable accuracy. Automating such tuning is not completely straightforward in a four-dimensional space. Furthermore, for some of the more extreme (but still experimentally interesting) combinations of input parameters, it may be difficult if not practically impossible to obtain converged solutions. Fortunately, in these cases, analytic asymptotic analysis may be used.

In this paper, by combining numerical and analytical results, a parametrization of the surface impedance for rf sheaths over the complete four-dimensional space is obtained. The method is to first obtain analytic results in the asymptotic cases, and then combine these results using Padé and other analytic interpolations into smooth functional forms that apply everywhere. Order unity coefficients are introduced into the interpolations and the value of these coefficients are determined by best fits to numerical results in the intermediate regimes. The end result is a fast, robust and easily implemented analytic expression for the sheath impedance that is applicable for any set of input parameters. The obtained functional fits are also continuously differentiable. This property can be important for some numerical implementations: the input parameters to the sheath model vary along the sheath surface, and high order numerical methods may require similar high-order smoothness in the BC. Another benefit of the analytical asymptotic approach is that physical insights into the final results are sometimes more apparent.

Our paper extends results that were briefly summarized in one section of an earlier conference report.²⁸ In Sec. II the basic sheath model of Ref. 26 is recapitulated. Voltage rectification and properties of a static biased sheath are also discussed and fitting functions are presented. Section III presents the derivation of the fitting functions for the electron, displacement and ion admittance (the inverse of the impedance). The numerical procedure for determining best-fit coefficients for all of these functions is presented in Sec. IV. Finally Sec. V gives a summary and conclusions.

II. The magnetized rf sheath model

In this paper all results will be presented in dimensionless variables where time is normalized to a reference upstream inverse ion plasma frequency $1/\omega_{pi0}$ and spatial dimensions

are normalized to a reference electron Debye length λ_{de0} . The density is normalized to the upstream density n_{i0} where the plasma is quasi-neutral, and rf voltages are normalized to T_e/e where T_e is the electron temperature, assumed to be constant. These units are natural ones for sheath dynamics, and result in velocities normalized to the ion sound speed $c_s = \lambda_{de}\omega_{pi}$. The corresponding dimensional equations and sheath impedance are given in Ref. 26.

The geometry under consideration is shown in Fig. 1. The fundamental equations of the sheath model are Poisson's equation for the electrostatic potential Φ , the Maxwell-Boltzmann relation for electron density n_e , the continuity equation for ion density n_i , and the three components of the ion equation of motion under the Lorentz force:

$$\frac{\partial^2 \Phi}{\partial x^2} = -(n_i - n_e) \quad (1)$$

$$n_e = \exp(\Phi - \Phi_0) \quad (2)$$

$$\frac{\partial n_i}{\partial t} + \frac{\partial}{\partial x}(n_i u_x) = 0 \quad (3)$$

$$\left(\frac{\partial}{\partial t} + u_x \frac{\partial}{\partial x} \right) u_x = -\frac{\partial \Phi}{\partial x} + \Omega u_p \quad (4)$$

$$\left(\frac{\partial}{\partial t} + u_x \frac{\partial}{\partial x} \right) u_p = \Omega u_{\parallel} b_x - \Omega u_x \quad (5)$$

$$\left(\frac{\partial}{\partial t} + u_x \frac{\partial}{\partial x} \right) u_{\parallel} = -\frac{\partial \Phi}{\partial x} b_x \quad (6)$$

Here $\Phi_0(t)$ is an upstream boundary condition on the potential (applied at the center of the domain in Fig. 1) that will be discussed shortly, \mathbf{u} is the ion velocity, with components (see Fig. 1) $u_x = \mathbf{e}_x \cdot \mathbf{u}$, $u_p = \mathbf{u} \cdot \mathbf{b} \times \mathbf{e}_x$, and $u_{\parallel} = \mathbf{u} \cdot \mathbf{b}$ where $\mathbf{b} = \mathbf{B}/B$ is the direction of the magnetic field. Note that $\mathbf{b} \times \mathbf{e}_x$ is not a unit vector in general. Also $b_x = \mathbf{e}_x \cdot \mathbf{b}$ and Ω is the ion magnetization parameter. In dimensional units $\Omega = \Omega_i/\omega_{pi} = \lambda_{de}/\rho_s$ where $\rho_s = c_s/\Omega_i$ is the ion sound radius. The size of the non-neutral Debye sheath relative to the quasi-neutral magnetic presheath is determined by Ω for rf sheaths, as it is for the more commonly studied case of static oblique angle magnetized sheaths.²⁹⁻³²

The model is driven by out-of-phase oscillating voltages at each plate

$$\Phi(x_1) = V_1 = \frac{V_{pp}}{2} \cos \omega t \equiv \xi \cos \varphi \quad (7)$$

$$\Phi(x_2) = V_2 = -\frac{V_{pp}}{2} \cos \omega t \equiv -\xi \cos \varphi \quad (8)$$

where V_{pp} is the peak-to-peak amplitude, ξ is the zero-to peak amplitude and $\varphi = \omega t$ is the wave phase. The current continuity equation at the plates is

$$J_{x1} - J_{x2} = 0 \quad (9)$$

where

$$J_{x1} = n_{i1}u_{x1} + \mu b_x \exp(V_1 - \Phi_0) - \frac{\partial^2 \Phi_1}{\partial t \partial x} \quad (10)$$

and for the symmetric double plate sheath model J_{x2} is obtained by the symmetry relation $J_{x2}(\omega t) = -J_{x1}(\omega t + \pi)$. Here μ is a constant given for deuterium by

$$\mu = \left(\frac{m_i}{2\pi m_e} \right)^{1/2} = 24.17 \quad (11)$$

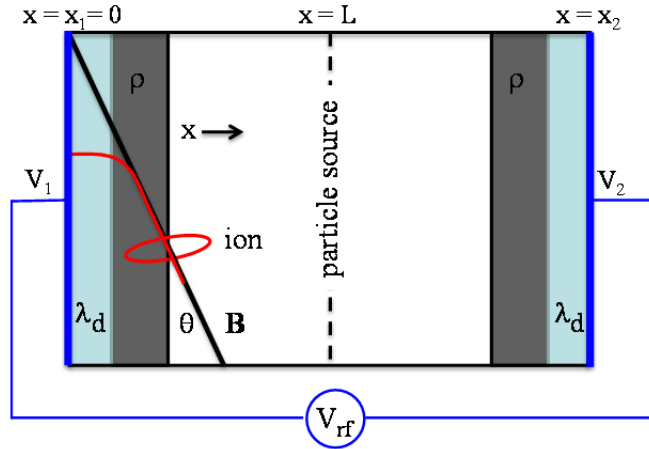


Fig. 1. Symmetric dual plate rf sheath model. A particle source is located at $x = L$ where the imposed ion parallel flow velocity towards the plates is taken to be greater than or equal to the sound speed.

As a consequence of Eqs. (9) and (10) together with symmetry, no time-averaged current may leave either plate, and hence there is no dc current flow from one plate to the other. The present

model implies complete voltage rectification of the applied rf field. The possibility of asymmetric sheaths which admit a dc current flow through the plasma that is completed in an external circuit is a very interesting one,^{33,34} but beyond the scope of the present study. The condition for vanishing dc current at x_1 , may be written as

$$u_{x0} + \mu b_x \langle \exp(V_1 - \Phi_0) \rangle = 0 \quad (12)$$

where $\langle \dots \rangle$ implies a time-average over an rf cycle, use has been made of the time-averaged ion continuity equation, $\langle n_i u_x \rangle = \text{constant} = u_{x0}$; the normalized upstream density is unity and u_{x0} is an upstream boundary condition on the ion flow.

In the dual plate model, a particle source is located at $x = L$ where the imposed ion parallel flow velocity is taken to be great than or equal to the sound speed, $u_{\parallel 0} \geq 1$. In this work we take

$$u_{x0} = b_x u_{\parallel 0} \quad (13)$$

It was shown in Ref. 26 and is clear from the model, that apart from the standard Bohm sheath boundary conditions on \mathbf{u}_0 all results of the model will depend at most on the four parameters

$$\omega, \Omega, b_x, \xi$$

A. Voltage rectification

In the present model, the upstream potential $\Phi_0(t)$ is determined by Eqs. (9), (10) and the symmetry relation $J_{x2}(\varphi) = -J_{x1}(\varphi + \pi)$. The time-averaged quantity $\langle \Phi_0 \rangle$ is the dc or ‘‘rectified’’ potential of the plasma with respect to the wall (i.e. the plate). Note that $\langle \Phi_0 \rangle$ contains the contribution of the usual thermal sheath, even in the absence of any rf driving voltage.

An analytic result for $\langle \Phi_0 \rangle$ is possible in the low frequency limit where the displacement current in Eq. (10) is negligible. In this case the equation for Φ_0 is

$$e^{-\Phi_0} = \frac{-n_{i1} u_{x1}}{\mu b_x \cosh(\xi \cos \varphi)} \quad (14)$$

where the symmetry relation $\Phi_0(\varphi) = \Phi_0(\varphi + \pi)$ has been used.²⁶ In the low frequency limit, the time derivative in the ion continuity equation may be neglected, resulting in the approximation $n_{i1} u_{x1} = u_{x0}$ which is independent of time. Using Eq. (13) and estimating $u_{\parallel 0} \approx -1$ inside the logarithm, the approximate result is

$$\Phi_0 = \ln[\mu \cosh(\xi \cos \varphi)], \quad \omega \ll 1 \quad (15)$$

From this waveform, $\langle \Phi_0 \rangle$ can be calculated numerically for given μ and ξ by performing the periodic average over φ . It can be shown that the small and large ξ limits are

$$\langle \Phi_0 \rangle = \begin{cases} \ln \mu, & \xi \ll 1, \omega \ll 1 \\ \ln(\mu/2) + \frac{2\xi}{\pi}, & \xi \gg 1, \omega \ll 1 \end{cases} \quad (16)$$

In the opposite, high frequency limit $\omega \gg 1$, the displacement current cannot be neglected, and the waveform given in Eq. (15) is no longer valid; however, the time-averaged total current constraint of Eq. (12) still applies. Numerical results²⁶ indicate that the waveform in this regime is approximately of the form $\Phi_0 = \langle \Phi_0 \rangle + \Phi_{02} \cos 2\omega t$. The second harmonic amplitude, like $\langle \Phi_0 \rangle$ is proportional to ξ but with a smaller coefficient. A very rough approximation for $\langle \Phi_0 \rangle$ may be obtained by neglecting Φ_{02} , which yields $\langle \Phi_0 \rangle = \ln[\mu I_0(\xi)]$ where I_0 is a Bessel function. This result has similar asymptotic forms to Eq. (16) but with a different coefficient of ξ in the large ξ limit.

Motivated by these limiting cases, a candidate analytic form for the rectified potential is taken as

$$\langle \Phi_0 \rangle = F[g(\omega)\xi] \quad (17)$$

where

$$F(\xi) = \frac{1}{2\pi} \int_0^{2\pi} d\varphi \ln[\mu \cosh(\xi \cos \varphi)] \quad (18)$$

and

$$g(\omega) = c_0 + c_1 \tanh(\omega) \quad (19)$$

The coefficients c_0 and c_1 will be determined by best fits to numerical data in Sec. IV. This form insures correct results for $\xi \rightarrow 0$, and with proper choice of coefficients, can match $\xi \gg 1$ results in both low and high frequency regimes. For convenient and fast numerical implementation, a Padé approximation to the integral in Eq. (18) is given in Appendix A.

B. Static biased sheath properties

Voltage rectification results in an rf sheath structure that shares some important properties with those of a similarly biased static sheath. This fact is anticipated from the capacitive sheath models,²²⁻²⁵ where the effective sheath capacitance is determined by the time-averaged sheath width as calculated from the time-averaged dc sheath potential drop. In this

section, static biased sheath properties are summarized. The results obtained here will be very useful in characterizing the rf properties discussed in Sec. III.

A comprehensive treatment of static strongly biased oblique-angle magnetized sheaths in asymptotic regimes satisfying $\Phi \gg 1$ and $\Omega \ll 1$ has been given by Ahedo.³⁵ In that work n_e , being exponentially small in the non-neutral sheath, was neglected and Φ was regarded as an applied bias, so the BC on the net current is not applicable. Using the remaining equations of the model, three asymptotic regimes were identified: $\Omega^4\Phi \ll b_x^2$, $b_x^2 \ll \Omega^4\Phi \ll 1$ and $1 \ll \Omega^4\Phi$. The corresponding non-neutral sheath width Δ was obtained by rigorous asymptotic analysis in each regime.

Here we are primarily interested in the scaling dependencies of various sheath quantities with the fundamental parameters of the static model, Ω , b_x , Φ . In each regime, appropriate simplifications may be made to the static version of Eqs. (1) and (3)–(6). From these, the scaling of Δ as well as ion density at the wall n_{iw} and the components of \mathbf{u} at the wall may easily be deduced. Results are summarized in Table 1 where we have set $u_{x0} \sim b_x$. In all regimes $u_x = b_x/n_i$ and is therefore not explicitly listed in the table. These estimates agree with Ref. 35, in as much as they are explicitly given there, if proper account is take of differences in normalizations. (In particular Ref. 35 adopts a presheath density normalization which differs by a factor of b_x from that employed here.)

Table I. Scaling of static biased sheath quantities.

Regime	Δ	n_{iw}	$u_{ }$	u_p
$\Omega^4\Phi \ll b_x^2$	$\frac{\Phi^{3/4}}{b_x^{1/2}}$	$\frac{b_x}{\Phi^{1/2}}$	$b_x u_x$	$b_y^2 \Omega \Delta$
$b_x^2 \ll \Omega^4\Phi \ll 1$	$\frac{\Phi^{1/2}}{\Omega}$	Ω^2	$\frac{b_x \Phi}{u_x}$	$\Omega \Delta$
$1 \ll \Omega^4\Phi$	$\Phi^{3/4}$	$\frac{1}{\Phi^{1/2}}$	$\frac{u_x}{b_x}$	$\frac{b_y^2 \Phi}{\Omega \Delta}$

The results given in Table 1 acquire a more uniform appearance when expressed in terms of the combination $\Omega_\Phi = \Omega\Phi^{1/4}$. It is not difficult to come up with approximate Padé rational expressions that uniformly describe all the regimes. In fact, once a Padé rational has been

determined for n_{iw} all the other quantities of interest may be obtained from it. Simple Padé rationals that give the correct asymptotic scalings are

$$n_{iw} = \frac{1}{\Phi^{1/2}} \frac{b_x + \Omega_{\Phi}^2}{1 + \Omega_{\Phi}^2} \quad (20)$$

$$\Delta = \left(\frac{\Phi}{n_i} \right)^{1/2} \quad (21)$$

$$u_x = \frac{b_x}{n_i} \quad (22)$$

$$u_{||} = n_i \Phi \quad (23)$$

$$u_p = \frac{b_y^2 \Omega \Delta}{1 + \Omega_{\Phi}^2} \quad (24)$$

These approximate expressions are also appropriate to describe the totally magnetized case $\Omega \gg 1$, which is technically not covered by the asymptotic analysis in Ref. 35. Note from Eq. (21) that the usual Child-Langmuir law is obtained for perpendicular sheaths ($b_x = 1$) and that Φ is of order unity or larger because of the thermal sheath which has $\Phi \sim 3$.

It is important to note that the density and velocity estimates are made at the wall and that Φ is the potential drop across the non-neutral sheath. If a neutral magnetic presheath is present, that presheath potential drop must be subtracted off before applying these results.

For more quantitatively accurate fits to the numerical results in Sec. IV, the preceding are generalized to

$$n_{iw}(\Omega, b_x, \Phi) = \frac{d_0}{d_2 + \Phi_d^{1/2}} \left(\frac{b_x^2 + d_4 + d_1^2 \Omega_{\Phi}^{2\nu_1}}{1 + d_4 + d_1^2 \Omega_{\Phi}^{2\nu_1}} \right)^{1/2} \quad (25)$$

$$\Phi_d = \Phi - \Phi_{ps}(b_x, \Omega) \quad (26)$$

$$\Omega_{\Phi} = \Omega \Phi_d^{1/4} \quad (27)$$

$$d_4 = d_2^2 / (\mu^2 d_0^2 - d_2^2) \quad (28)$$

where d_0, d_1, d_2 and v_1 are constants to be fit and d_4 is chosen to make $n_i = 1/\mu$ in the limit $b_x \rightarrow 0$ and $\Omega_\Phi \rightarrow 0$. In this limit the non-neutral sheath vanishes, hence $\Phi_d = 0$ and also $n_e = 1/\mu$ and $\Phi_{ps} = \ln \mu$ (See following.) Here, Φ from Eqs. (20) – (24) is now explicitly replaced by Φ_d , the potential drop across the non-neutral Debye sheath, and Φ_{ps} is the potential drop across the magnetic pre-sheath. The latter quantity is approximately given by

$$\Phi_{ps}(b_x, \Omega) = -\frac{1}{1+d_3\Omega^2} \ln\left(\frac{\mu^2 b_x^2 + 1}{\mu^2 + 1}\right)^{1/2} \approx \frac{-\ln b_x}{1+d_3\Omega^2} \quad (29)$$

valid for valid for $b_x \gg 1/\mu \approx 0.041$. Here $0 < d_3 < 1$ is a constant to be determined by fitting. The $\ln b_x$ factor is readily understood from the drop in density associated with the acceleration of u_x from $u_{x0} = O(b_x)$ to order unity across the magnetic pre-sheath. Using $n_i u_x = \text{constant}$, and the Boltzmann relation connecting (quasi-neutral) density and potential results in the $\ln b_x$ factor. The denominator describes the fact that for $\Omega \gg 1$, there is no magnetic presheath.

Other quantities of interest may be obtained from n_{iw} with additional multiplicative fit factors:

$$\Delta = e_0 \left(\frac{\Phi_d}{n_{iw}} \right)^{1/2} \quad (30)$$

$$u_x = -e_1 \frac{b_x}{n_{iw}} \quad (31)$$

$$u_{||} = -e_2 (1 + n_{iw} \Phi_d) \quad (32)$$

While the form of Eqs. (30) – (32) can be deduced from the original differential equations by replaced d/dx with $1/\Delta$, the same procedure does not work well for u_p because each equation with u_p has terms which can cancel in some regimes (making subtraction of approximate forms inaccurate). For u_p we consider a separate numerical fit to the form

$$u_p = f_0 \frac{b_y^2 \Omega \Delta}{\left(1 + f_1 \Omega_\Phi^{2\nu_2}\right)^{1/\nu_2}} \quad (33)$$

where f_0 , f_1 , and v_2 are fit parameters. Equations (30) – (33) are given for completeness in characterizing the static biased sheath, but are not used directly in the following; on the other hand Eqs. (25) – (29) are important for subsequent analysis.

III. Contributions to the rf sheath admittance

At sufficiently large distances from the Debye sheath, the electric field $E_x = -\partial\Phi/\partial x$ usually vanishes and the voltage drop across the sheath is well defined. (An exception occurs in a few cases where the sheath launches propagating waves; this situation will be discussed in Sec. IV.) The plasma responds to the sheath voltage drop with an rf current across the sheath. The total current (electron, displacement and ion) must have zero divergence from Maxwell's equations, and therefore can be evaluated at any convenient point: here we choose the wall. The (normalized) sheath admittance y is defined as the ratio of rf current density to the rf potential across the sheath at frequency ω , and its inverse is the (normalized) sheath impedance z . The following Fourier projection operation extracts the desired result²⁶

$$y = \frac{1}{z} = \frac{\langle J\mathcal{V} \rangle}{\langle \mathcal{V}^2 \rangle} - \frac{i\omega \langle J\dot{\mathcal{V}} \rangle}{\langle \dot{\mathcal{V}}^2 \rangle} \quad (34)$$

where J is the total current, $\dot{\mathcal{V}} = d\mathcal{V}/dt$ and all quantities are evaluated at the wall $x = x_1$. Thus the total admittance can be written as the sum of electron, displacement and ion admittances

$$y = y_e + y_d + y_i \quad (35)$$

Each of these will be evaluated separately in the following

A. Electron admittance

Because the electrons are assumed to obey the Maxwell-Boltzmann relation, their contribution to the admittance may be evaluated almost completely analytically. The electron current at the plate is given by

$$J_{e1} = \mu b_x e^{\xi \cos \varphi - \Phi_0} \quad (36)$$

Thus the electron admittance is

$$y_e = \frac{2\langle J_{e1} \cos \varphi \rangle}{\xi} + \frac{2i\langle J_{e1} \sin \varphi \rangle}{\xi} \quad (37)$$

The imaginary part of y_e vanishes because Φ_0 and hence J_{e1} is an even function of φ . The remaining real part is

$$y_e = \frac{2\mu b_x}{\xi} \left\langle \cos\varphi e^{\xi \cos\varphi - \Phi_0} \right\rangle \quad (38)$$

To proceed further it is necessary to know $\Phi_0(t)$. This fact emphasizes the sensitivity of the electron impedance to the voltage rectification model and harmonic generation, and hence to the complete global circuit. For the symmetric dual plate model, using Φ_0 in the low frequency limit from Eq. (15) gives

$$y_e = \frac{4b_x}{\xi} \left\langle \frac{\cos\varphi}{1 + e^{-2\xi \cos\varphi}} \right\rangle \equiv b_x H_e(\xi) \quad (39)$$

This result is rigorous when the time-dependent ion and displacement currents can be neglected in the evaluation of Φ_0 . This is the limit in which the electron admittance is dominant and is therefore of most interest. For power absorption considerations, however, y_e may also be of interest in the large ω (capacitive) limit where y_e does not dominate y but it does dominate the power absorption. In general, y_e should be linear in b_x , weakly dependent on ω , and independent of Ω . It can be shown that H_e defined implicitly by Eq. (39) has the following asymptotic limits

$$H_e = \begin{cases} 1, & \xi \ll 1 \\ \frac{4}{\pi\xi}, & \xi \gg 1 \end{cases} \quad (40)$$

The fitting function for the electron admittance is taken to be

$$y_e = h_0 b_x H_e(\xi) \quad (41)$$

where the constant h_0 will be determined by best fits to numerical data in Sec. IV. For convenient and fast numerical implementation, a Padé approximation to $H_e(\xi)$ is given in Appendix A.

B. Displacement admittance

The form of the displacement admittance is the same as in the capacitive sheath model

$$y_d = -s_0 \frac{i\omega}{\Delta} \quad (42)$$

except now the time-averaged sheath width Δ must be computed for general parameters. Here s_0 is a fitting coefficient to be determined. The time-averaged non-neutral sheath width is primarily

set by the dc potential drop across the sheath, thus the scaling of Δ should be identical to that of a similarly biased static sheath, as given by Eq. (30). A slight improvement in the fits to be discussed in Sec. IV was obtained by allowing for a small frequency dependence in n_{iw} , which in Eq. (25) is given for the static case. The modified form is given by

$$n_{iw\omega}(\omega, \Omega, b_x, \xi) = n_{iw}(\Omega, b_x, \Phi') \quad (43)$$

where

$$\begin{aligned} \Phi' &= \Phi_s + (\langle \Phi_0 \rangle - \Phi_s) \tanh \omega \\ \Phi_s &= k_0 + k_1 (\xi - k_0) \end{aligned} \quad (44)$$

k_0 and k_1 are fitting coefficients and $\langle \Phi_0 \rangle$ is given by Eq. (17). Then the effective sheath width is computed from

$$\Delta = \left(\frac{\langle \Phi_0 \rangle}{n_{iw\omega}} \right)^{1/2} \quad (45)$$

and y_d is given by Eq. (42). Equations (43) – (45) generalize Eq. (25), obtained for static sheaths, to allow for a weak frequency dependence in the rf-cycle-averaged ion density at the wall.

C. Ion admittance

The ion admittance is the most complicated to characterize because the ion dynamics is influenced by both the electric and magnetic parts of the Lorentz force for oblique magnetic field lines. Some insight into the ion dynamics can be gained by first examining the case $b_x = 1$ where the magnetic field is perpendicular to the surface and hence there is no magnetic force on the ions. Fits for the ion admittance in this case, accurate to a few percent, were given in Ref. 36 and properties of the global wave solutions for perpendicular incidence are discussed there and in Ref. 28. Figure 2 illustrates the dependence of y_i on the frequency.

From Fig. 2, it will be seen that near $\omega \sim 1$ a broad resonance feature exists where the real part of y_i maximizes and the imaginary part changes sign. Near the resonance, the ions traverse the Debye sheath in a time of order unity that is comparable to the wave period. There are very few charge-neutralizing electrons in the Debye sheath, therefore the electrostatic ion plasma resonance is exposed. (Recall that $\omega \sim 1$ corresponds to $\omega \sim \omega_{pi}$ in dimensional units.) At large rf voltages, and hence large rectified voltages, the ion density in the sheath is reduced, according to Eq. (25) or (43); this reduces the effective value of ω_{pi} in the sheath and hence reduces the resonant frequency as seen in the figure. The reduced ion density also implies a reduced ion current to the plate, and hence a reduced peak amplitude of $|y_i|$.

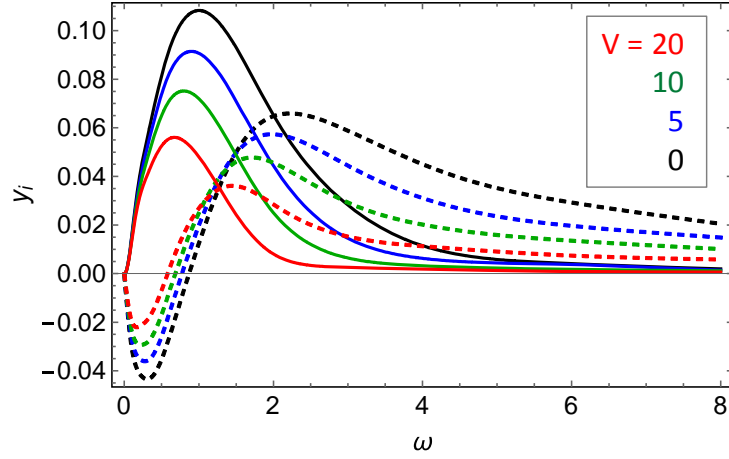


Fig. 2. The dependence of the ion admittance y_i on frequency and rf voltage for perpendicular incidence, using the fits given in Ref. 36. $\text{Re}(y)$ is shown with solid lines and $\text{Im}(y)$ with dashed lines. $V = 2\xi$ is the normalized peak-to-peak rf voltage.

For the general oblique magnetized case, additional insight may be obtained by exploring the limiting cases of low and high frequency. The high frequency case $\omega \gg 1$ is considered first. In the high frequency regime the “immobile” ions have only a small rf response, and background flows can be neglected ($\partial_t \gg u_x \partial_x$) in the fundamental equations. As a result the dynamics are linear and the governing equations are

$$-i\omega\tilde{n}_i + \partial_x(n_i\tilde{u}_x) = 0 \quad (46)$$

$$-i\omega\tilde{u}_x = -\partial_x\tilde{\Phi} + \Omega\tilde{u}_p \quad (47)$$

$$-i\omega\tilde{u}_p = \Omega(b_x\tilde{u}_{\parallel} - \tilde{u}_x) \quad (48)$$

$$-i\omega\tilde{u}_{\parallel} = -b_x\partial_x\tilde{\Phi} \quad (49)$$

Here the over-tilde indicates the response at frequency ω . Eliminating variables leads to

$$\tilde{u}_x = \frac{-ig}{\omega}\partial_x\tilde{\Phi} \quad (50)$$

where

$$g = \frac{\omega^2 - b_x^2\Omega^2}{\omega^2 - \Omega^2} \quad (51)$$

Note that for ICRF applications, $g \approx 1$ frequently applies since the ω^2 term usually dominates in both the numerator and denominator, particularly in the low-field-side edge plasma. In the high frequency regime one has, $\tilde{n}_i/n_i \ll \tilde{u}_x/u_x$ where we estimate $\partial_x \tilde{\Phi} \sim 1/\Delta$ and use the fact that $u_x \ll \omega\Delta$. As a result the ion current and the ion impedance are

$$\tilde{J}_i = n_i \tilde{u}_x \quad (52)$$

$$y_i = \frac{\tilde{J}_i}{\tilde{\Phi}} = -i \frac{gn_i}{\omega} \frac{\partial_x \tilde{\Phi}}{\tilde{\Phi}} \quad (53)$$

The scaling and sign of y_i in the high frequency regime is given by noting that $\partial_x \tilde{\Phi}/\tilde{\Phi} \approx -1/\Delta$, thus a scaling estimate is given by

$$y_i \approx i \frac{gn_i}{\omega\Delta} \approx i \frac{gn_i^{3/2}}{\omega\Phi^{1/2}} \quad (54)$$

Here n_i should be calculated using the dc sheath model with the appropriate dc bias potential.

The other limit that can be estimated from analytical analysis is the low frequency limit $\omega \ll 1$. In the low frequency regime, at each point in the time cycle of the rf, the ions respond as if the applied voltage were static. The leading ω dependence of the ion admittance comes from the explicit ω in the continuity equation

$$\tilde{J}_i = -i\omega \int_0^\Delta dx \tilde{n}_i \approx -i\omega\Delta\tilde{n}_i \quad (55)$$

where we define impedance at the fundamental rf frequency, but retain nonlinearities in the evaluations. Specifically, the super-tilde here indicates the ω Fourier component, but linearization is not implied. It remains to determine the phase relationship and scaling of n_i with respect to Φ in order to obtain $y_i = \tilde{J}_i/\tilde{\Phi}$. This is immediately obtained from the static biased sheath results in Sec. II B, in particular Eq. (21). Combining with Eqs. (55) and (56)

$$y_i \approx -i\omega \frac{\Delta n_i}{\Phi} \approx -i \frac{\omega n_i^{1/2}}{\Phi^{1/2}} \quad (56)$$

It also possible to make a rough estimate of the amplitude of y_i at resonance. At resonance the ion travel time across the non-neutral sheath is comparable to the wave period, thus one expects ∂_t and $u_x \partial_x$ to be comparable in Eqs. (3) – (6). The width of the resonance in frequency space should be of order $\gamma \sim u_x/\Delta$. Furthermore, at resonance the difference $\partial_t - u_x \partial_x$

may be estimated of order γ . Thus a rough estimate of the amplitude of y_i at resonance is obtained from Eq. (54) by replacing $-i\omega$ with γ and estimating $g \sim 1$.

$$y_{ir} \approx \frac{n_i}{\gamma\Delta} \approx \frac{n_i}{u_x} \approx \frac{n_i^2}{b_x} \quad (57)$$

where $u_x = b_x/n_i$ has been used.

The preceding scalings of the ion impedance are smoothly captured by the expression

$$\tilde{y}_i \approx \frac{ip_0\tilde{\omega}}{\tilde{\omega}^2/g - p_1 + ip_2\tilde{\gamma}\tilde{\omega}} \quad (58)$$

where

$$y_i \equiv \frac{n_{iw\omega}}{\langle\Phi_0\rangle^{1/2}} \tilde{y}_i \quad (59)$$

$$\tilde{\omega} \equiv p_3\omega/n_{iw\omega}^{1/2} \quad (60)$$

$$\tilde{\gamma} = \frac{b_x}{n_{iw\omega}\langle\Phi_0\rangle^{1/2}} \quad (61)$$

and p_0, p_1, p_2, p_3 are order unity constant coefficients to be determined by fits to numerical data; $n_{iw\omega}$ is given by Eq. (43) and $\langle\Phi_0\rangle$ by Eq. (17). The case of ion cyclotron resonance, $\omega = \Omega$, where $g \rightarrow \infty$ may require further study; however, even in this case Eq. (58) remains well posed. The ion plasma resonance, where the denominator is pure imaginary, is at $\tilde{\omega} \approx g^{1/2}$. For $g \sim 1$, this gives $\omega \sim n_{iw\omega}^{1/2}$ where $n_{iw\omega}^{1/2}$ is the dimensionless ion plasma frequency in the non-neutral sheath. Other limits are also sensible. For example in the strongly magnetized regime $\Omega \rightarrow \infty$ one obtains $g^{1/2} = b_x$ from Eq. (51). In this case the resonance condition is $\omega \sim b_x n_{iw\omega}^{1/2}$; here, $b_x n_{iw\omega}^{1/2}$ is the normalized ion plasma frequency obtained by employing an effective ion mass $m_i^* = m_i/b_x^2$. The effective mass treatment of strongly magnetized particles in the sheath has been noted previously.³⁷

IV. Numerical fits and accuracy testing

In Sec. III physics-based functional forms were obtained for the electron, displacement and ion contributions to the admittance. In this section, numerical data is employed to determine best fits to the free coefficients in these expressions. Because the physics based functional forms make explicit the most important parametric dependencies and the corresponding parameter

ranges where admittance variations are expected, the free coefficients can be determined from judicious parameter scans without having to sample the entire four-dimensional parameter space.

The database chosen for the fits presented here was obtained from 497 numerical evaluations of y_e , y_d , y_i and their sum y using the method described in Ref. 26. The numerical inaccuracy of these evaluations is estimated at no more than 5% in most cases, limited by resolution of the space-time grid. In some cases, particularly at small b_x , the sheath can launch waves which propagate upstream and create additional numerical accuracy issues; these and other caveats are discussed in Sec. V. The database sampled 23 different values of ω ranging from 0.001 to 9; 17 different values of Ω ranging from 0.001 to 1 (large Ω behavior was already evident for $\Omega = 1$); 4 different values of b_x ranging from 0.1 to 1; and 21 different values of ξ ranging from 0.001 to 10.

For each function, $\langle\Phi_0\rangle$, $n_{iW\omega}$, y_e , y_d , y_i and y , the free coefficients were determined by least-squares fits to the entire database. In the case of $n_{iW\omega}$, best fits for the coefficients in n_{iW} were first determined from a separate database for static sheaths, and then the remaining coefficients in $n_{iW\omega}$ were determined by an additional fit. Figures 3 – 8 illustrate the resulting quality of fits. In each case the solid blue line through the data points represents a perfect fit. The rms absolute error for each fit, denoted E_{rms} , is given in the corresponding figure caption and the best fit coefficients are given in Appendix A. E_{rms} is to be compared with the scale of each plot.

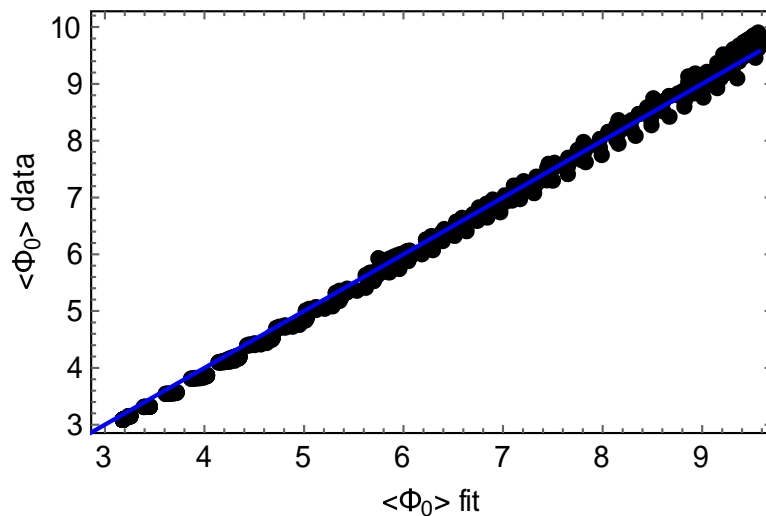


Fig. 3. Quality of fit for the rectified potential $\langle\Phi_0\rangle$; $E_{\text{rms}} = 0.11$.

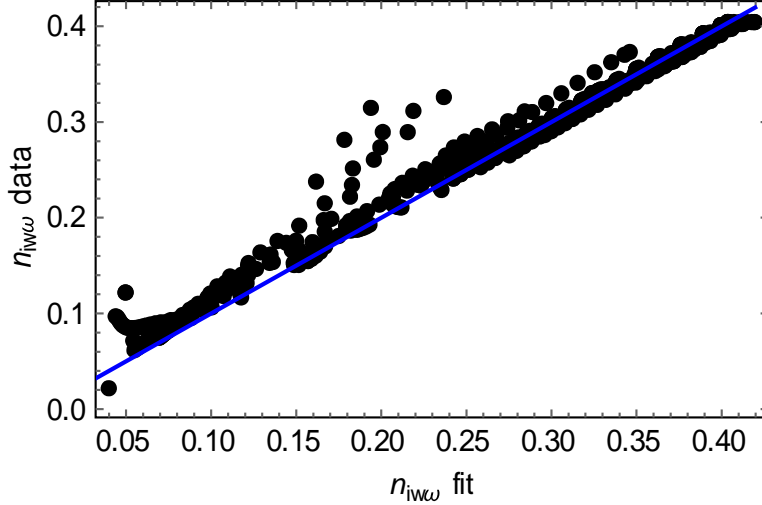


Fig. 4. Quality of fit for the ion density in the sheath $n_{i\omega}$; $E_{rms} = 0.016$.

While the fit for the rectified potential in Fig. 3 is quite good, the ion density in the sheath, shown in Fig. 4, has a few outliers. These outliers occur for some cases involving small values of $b_x = 0.1$ or 0.2 . In spite of the poor quality of the fits for those cases the effect on the displacement admittance, which depends on the square-root of this density, appears to be minimal, as shown in Fig. 6. As might be expected, the complex resonance structure of the ion admittance is the most difficult to fit. Results in Fig. 7 show that the major trends are captured. More significantly, note from the scale of the plot that y_i is quite small compared with y_e and y_d . Consequently, the net fit for the total impedance shown in Fig. 8 is quite acceptable.

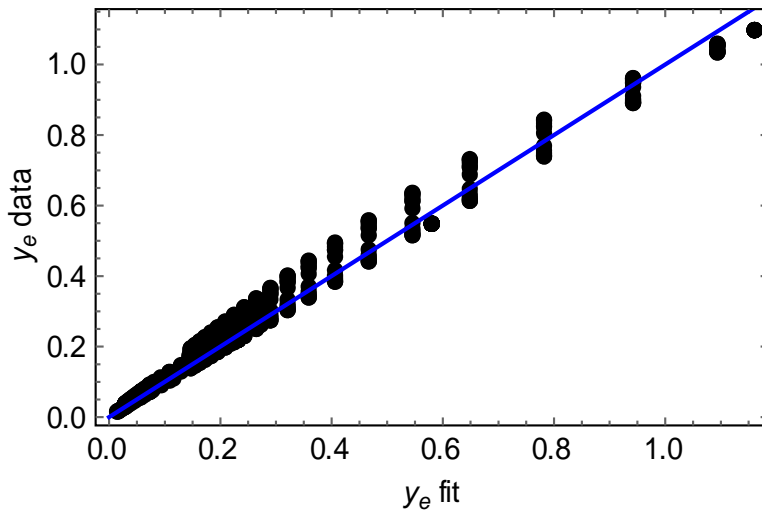


Fig. 5. Quality of fit for the electron admittance y_e ; $E_{rms} = 0.034$.

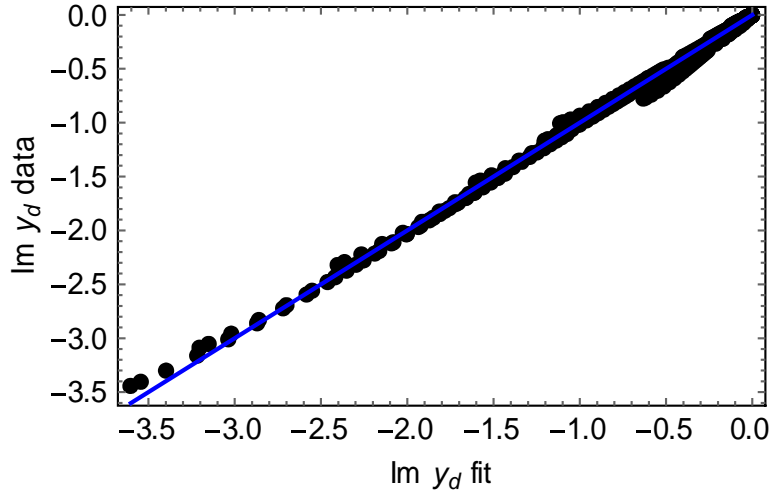


Fig. 6. Quality of fit for the displacement admittance y_d ; $E_{rms} = 0.033$.

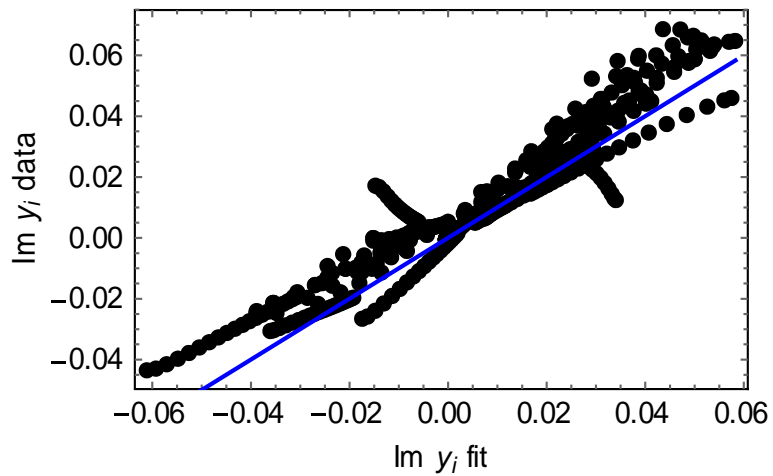
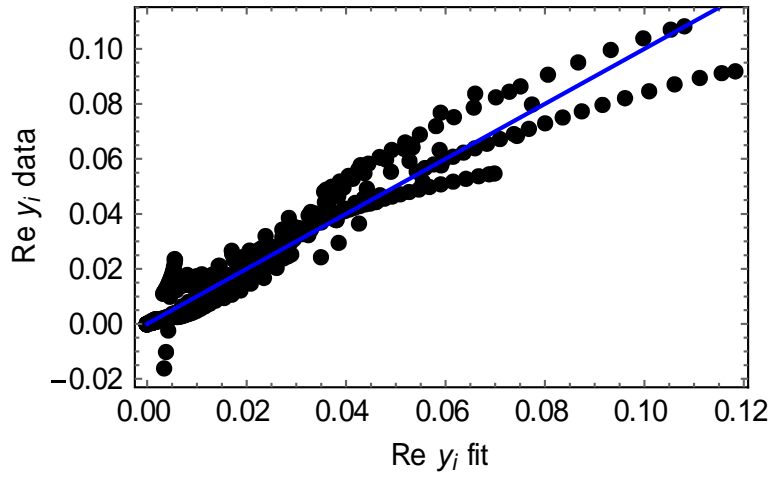


Fig. 7. Quality of fit for the real part of the ion admittance $Re y_i$ (upper panel), $E_{rms} = 0.006$; and for the imaginary part of the ion admittance $Im y_i$ (lower panel), $E_{rms} = 0.007$.

Obtaining a good parameterization of the total impedance is the primary goal of this work. Figure 8 shows no more than a 20% discrepancy at the largest values of $|y|$ and captures all the trends over order-of-magnitude or more variations in ω , Ω , b_x , and ξ . Given the limitations of the underlying physics model, this accuracy is quite sufficient. It is also useful to note that at the largest values of admittance, $|y| \gg 1$, the precise value of y that is employed as a BC in a global code is unimportant: for $|y| \gg 1$ the BC approaches the perfectly conducting limit and small deviations from perfectly conducting have little effect on the global wave solution.

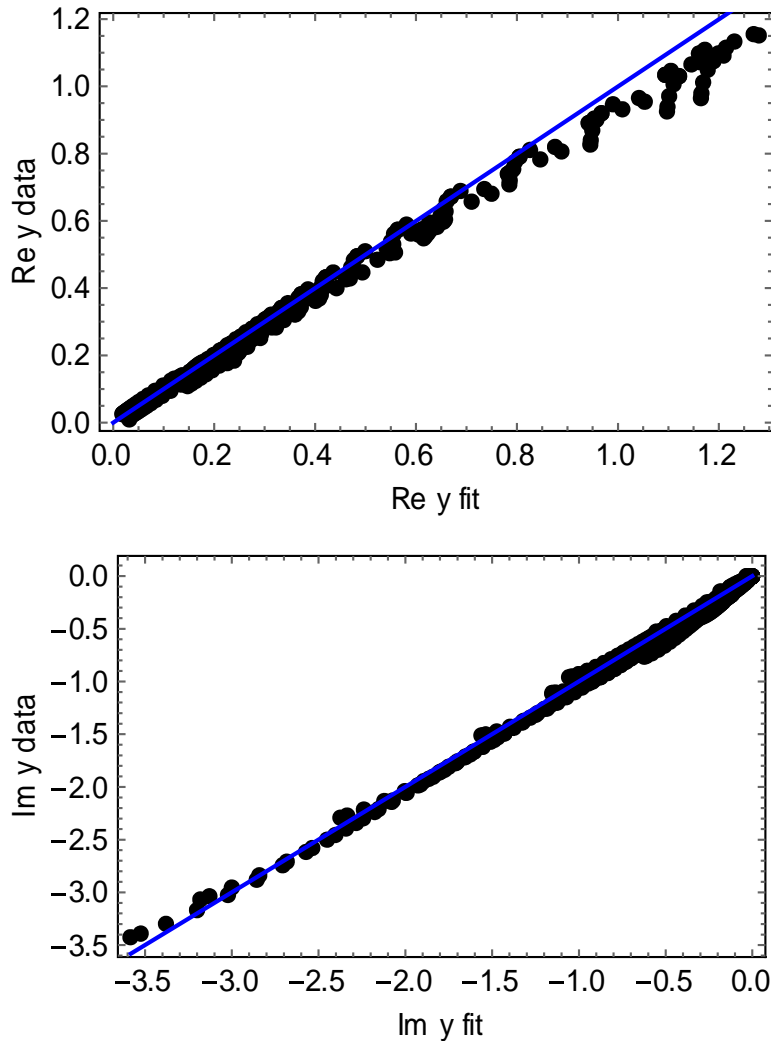


Fig. 8. Quality of fit for the real part of the total admittance $\text{Re } y$ (upper panel), $E_{\text{rms}} = 0.030.$; and for the imaginary part of the total admittance $\text{Im } y$ (lower panel), $E_{\text{rms}} = 0.043.$

V. Summary and conclusions

The primary results of this paper are to be found in Eqs. (17) – (19) for voltage rectification; Eqs. (25) – (28), (43) and (44) for the average ion density at the wall; Eqs. (41) and (42) for the electron and displacement admittance respectively; Eqs. (58) – (61) for the ion admittance; and trivially Eq. (35) for the total admittance. The best fits for the coefficients in these equations are given in Appendix A together with Padé fits for the functions $F(\xi)$ and $H_e(\xi)$.

The fidelity of the fits for the rectified potential and the total admittance is quite good as indicated in Figs. 3 and 8: a fit accuracy of better than 10% was achieved over all points tested; moreover, the parametrization method insures sensible results for *any* of combination of input parameters. The fits are smooth and continuously differentiable in all variables as required for implementation in high order discretization schemes. Many asymptotic limits of the sheath model are captured exactly by the parametrization. Furthermore, it is straightforward to embed this parametrization in a computer subroutine that is robust and fast. Further improvements in the fits is likely not warranted given the limitations of the physics model, as discussed next.

Although the present parametrization of the voltage rectification and sheath impedance (or admittance) is a significant improvement over the frequently employed and much simpler capacitive sheath model, the development of more sophisticated sheath impedance models is still needed. The assumption of Maxwell-Boltzmann electrons, made here, is unlikely to be valid for all interesting parameter ranges, and should fail when $\omega \geq b_x v_{te}/\Delta$ where v_{te} is the electron thermal velocity. Also, as discussed in Sec. II, sheaths that are asymmetrical at opposite ends of the field line can easily occur. For these, the model should be extended to allow for net dc current flow through the plasma in a circuit that is completed in the hardware (e.g. the antenna or tokamak wall). In this case, voltage rectification can be partly mitigated,³³ and as a result y_e , y_d , and y_i , which depend on $\langle \Phi_0 \rangle$, would be modified. The primitive forms of y_e , y_d , and y_i , before substituting for Φ_0 , should be useful for this purpose. Boundary conditions on the dc current and how one drives the system (with respect to second harmonic generation) will affect the results.

Another aspect of the model which may require further investigation is the launching of waves which propagate upstream from the sheath. This phenomenon is sometimes observed for small values of b_x and ω ($= \omega/\omega_{pi}$ in dimensional variables). In the present one-dimensional model, these waves can create numerical difficulties and potentially add fine structure to the sheath impedance. The physical importance of these waves in more realistic higher dimensional models is unclear at present. For example tangency points where $b_x \rightarrow 0$ are isolated (e.g. near a limiter tip) and plasma density may vary significantly along the curved surface, requiring a two-dimensional treatment. Some of the waves may be related to non-monotonic spatial oscillations that occur in the profiles of n_i and u_x for static biased sheaths in a cold ion model.³⁵ Wave

oscillations in the quasi-neutral static presheath, likely of a different origin, were also pointed out by Chodura.³⁰ Given these previous observations, it is not surprising that waves could be excited by an rf driven sheath.

Wave oscillations aside, the structure of sheaths (even dc sheaths let alone rf sheaths) for very shallow B-field angles, $b_x \rightarrow 0$, is complex³⁸⁻⁴² and still a subject of active investigation. This issue is important because near-tangency points are often where strong rf sheaths from (fast wave to slow wave) polarization conversion occur.⁴³ Furthermore, the sheath BC can introduce rapid, difficult-to-resolve structure in the solutions near a tangency point,⁴³ motivating a careful re-examination of the physical model.

Thus, remaining topics left for future work are improvements in the modeling of electron dynamics, asymmetrical sheaths, global circuits, sheath-induced wave oscillations, and tangency interactions. Despite these open topics, the present model should provide a significant improvement in the modeling of ICRF waves in the SOL plasma near material surfaces, allowing for the first time a practical treatment of resistive and capacitive sheath impedance effects on wave-boundary interactions for general geometric, rf and plasma parameters. This capability will permit an evaluation of global and local rf power dissipation through the sheath, as well as the rectified sheath voltage for calculation of ion impact energies for sputtering.

Acknowledgements

This material is based upon work supported by the U.S. Department of Energy Office of Science, Office of Fusion Energy Sciences under Award Numbers DE-FC02-05ER54823 and DE-FG02-97ER54392. Discussions with H. Kohno, E. D’Azevedo, and team members of the rf SciDAC project (Center for Simulation of Wave-Plasma Interactions) are gratefully acknowledged.

The digital data for this paper can be found at <http://doi.org/10.5281/zenodo.494983>.

Appendix A: Padé approximations and best fit coefficients

The integral in Eq. (18) is approximately given by

$$F(\xi) = \frac{a_0 + a_1\xi + a_2\xi^2 + a_3\xi^3}{1 + b_1\xi + b_2\xi^2} \quad (\text{A1})$$

where

$$\begin{array}{lll} a_0 = 3.18553 & a_1 = 3.70285 & a_2 = 3.81991 \\ a_3 = 2b_2/\pi & b_1 = 1.13352 & b_2 = 1.24171 \end{array}$$

This approximation is asymptotically correct to leading order for both small and large ξ and the maximum relative error over the range $0 < \xi < 10$ is 0.0016.

The best-fit coefficients in Eq. (19) for the function $g(\omega)$ are

$$c_0 = 0.966463 \quad c_1 = 0.141639$$

Here and throughout $\mu = 24.17$.

The best-fit coefficients to the expressions in Eqs. (25) – (33) for the static sheath properties are

$$\begin{aligned} d_0 &= 0.794443 & d_1 &= 0.803531 & d_2 &= 0.182378 \\ d_3 &= 0.995721 & d_4 &= 0.0000901 & v_1 &= 1.455592 \\ e_0 &= 0.718981 & e_1 &= 1.10822 & e_2 &= 1.43336 \\ f_0 &= 1.47923 & f_1 &= 0.800775 & v_2 &= 1.27038 \end{aligned}$$

The function $H_e(\xi)$ defined by Eq. (39) and used in calculating the electron admittance is approximately given by

$$H_e(\xi) = \frac{1 + h_1\xi + h_2\xi^2}{1 + g_1\xi + g_2\xi^2 + g_3\xi^3} \quad (\text{A2})$$

where

$$\begin{aligned} h_1 &= 0.607405 & h_2 &= 0.325497 \\ g_1 &= 0.624392 & g_2 &= 0.500595 & g_3 &= \pi h_2/4 \end{aligned}$$

This approximation is asymptotically correct to leading order for both small and large ξ and the maximum relative error over the range $0 < \xi < 10$ is 0.002.

The best-fit coefficients to the expressions in Eqs. (41), (42) and (44) for the electron and displacement admittance are

$$\begin{aligned} h_0 &= 1.161585 & k_0 &= 3.7616 & k_1 &= 0.22202 \\ s_0 &= 1.12415 \end{aligned}$$

The best-fit coefficients to the expressions in Eqs. (58) – (61) for the ion admittance are

$$\begin{aligned} p_0 &= 1.05554 & p_1 &= 0.797659 & p_2 &= 1.47405 \\ p_3 &= 0.809615 \end{aligned}$$

References

- ¹ J.-M. Noterdaeme and G. Van Oost, Plasma Phys. Control. Fusion **35**, 1481 (1993).
- ² J.R. Myra, D.A. D'Ippolito, D.A. Russell, L.A. Berry, E.F. Jaeger and M.D. Carter, Nucl. Fusion **46** S455 (2006).
- ³ D. A. D'Ippolito and J. R. Myra, J. Nucl. Mater. **415**, S1001- S1004 (2011).
- ⁴ S. J. Wukitch, M. L. Garrett, R. Ochoukov, J. L. Terry, A. Hubbard, B. Labombard, C. Lau, Y. Lin, B. Lipschultz, D. Miller, M. L. Reinke, D. Whyte, and Alcator C-Mod Team, Phys. Plasmas **20**, 056117 (2013).
- ⁵ V. Bobkov, M. Balden, R. Bilato, F. Braun, R. Dux, A. Herrmann, H. Faugel, H. Fünfgelder, L. Giannone, A. Kallenbach, H. Maier, H.W. Müller, R. Neu, J.-M. Noterdaeme, Th. Pütterich, V. Rohde, N. Tsujii, F. Zeus, H. Zohm and the ASDEX Upgrade Team, Nucl. Fusion **53**, 093018 (2013).
- ⁶ J. Jacquot, D. Milanesio, L. Colas, Y. Corre, M. Goniche, J. Gunn, S. Heuraux, and M. Kubi, Phys. Plasmas **21**, 061509 (2014).
- ⁷ C. M. Qin, Y. P. Zhao, H. Q. Wang, X. J. Zhang, B. N. Wan, J.-M. Noterdaeme, F. Braun, V. Bobkov, H. Kasahara, E. H. Kong, L. Wang, Y. Shuai, Z. X. He, B. J. Ding, ICRF Team and EAST Team, Plasma Phys. Control. Fusion **55**, 015004 (2013).
- ⁸ Y. Corre, M. Firdouss, L. Colas, A. Argouarch, D. Guilhem, J. Gunn, C Hamlyn-Harris, J. Jacquot, M. Kubic, X. Litaudon, M. Missirlian, M. Richou, G. Ritz, D. Serret and K. Vulliez, Nucl. Fusion **52**, 103010 (2012).
- ⁹ I. Cziegler, J. L. Terry, S. J. Wukitch, M. L. Garrett, C. Lau and Y. Lin, Plasma Phys. Control. Fusion **54**, 105019 (2012).
- ¹⁰ R.J. Perkins, J.-W. Ahn, R.E. Bell, A. Diallo, S. Gerhardt, T.K. Gray, D.L. Green, E.F. Jaeger, J.C. Hosea, M.A. Jaworski, B.P. LeBlanc, G.J. Kramer, A. McLean, R. Maingi, C.K. Phillips, M. Podesta, L. Roquemore, P.M. Ryan, S. Sabbagh, F. Scotti, G. Taylor and J.R. Wilson, Nucl. Fusion **53**, 083025 (2013).
- ¹¹ R. Ochoukov, D. G. Whyte, D. Brunner, D. A. D'Ippolito, B. LaBombard, B. Lipschultz, J. R. Myra, J. L. Terry and S. J. Wukitch, Plasma Phys. Control. Fusion **56**, 015004 (2014).
- ¹² K. Crombé, R. D'Inca, J. Jacquot, R. Ochoukov, M. Usoltceva, A. Kostic, F. Louche, D. Van Eester, A. Nikiforov, J. Moreno, S. Heuraux, S. Devaux, J. Moritz, E. Faudot, H. Fünfgelder, H. Faugel, F. Zeus and J.-M. Noterdaeme, "IShTAR: a helicon plasma source to characterise the interactions between ICRF and plasma," 26th IAEA Fusion Energy Conference, Kyoto, Japan, 17-22 October 2016, IAEA-CN-234/EX-P6-48.
- ¹³ M. Martin, W. Gekelman, P. Pribyl, B. Van Compernelle, T. Carter, D. Van Eester, K. Crombé, "Experimental Study of Convective Cells and RF Sheaths Excited by a Fast Wave Antenna in the LAPD," Bull. American Phys. Soc. **61**, 299, paper PP10-11.
- ¹⁴ L. Colas, J. Jacquot, S. Heuraux, E. Faudot, K. Crombé, V. Korytsya, J. Hillairet and M. Goniche, Phys. Plasmas **19**, 092505 (2012).
- ¹⁵ D. N. Smithe, D. A. D'Ippolito, and J. R. Myra, AIP Conference Proceedings **1580**, 89 (2014).
- ¹⁶ N. Bertelli, E.F. Jaeger, J.C. Hosea, C.K. Phillips, L. Berry, S.P. Gerhardt, D. Green, B. LeBlanc, R.J. Perkins, P.M. Ryan, G. Taylor, E.J. Valeo and J.R. Wilson, Nucl. Fusion **54**, 083004 (2014).

- ¹⁷ D. Van Eester, K. Crombé and V. Korytsya, *Plasma Phys. Control. Fusion* **55**, 055001 (2013).
- ¹⁸ J.R. Myra and D.A. D’Ippolito, *Plasma Phys. Controlled Fusion* **52**, 015003 (2010).
- ¹⁹ H. Kohno, J. R. Myra, and D. A. D’Ippolito, *Phys. Plasmas* **19**, 012508 (2012).
- ²⁰ D. A. D’Ippolito, J. R. Myra, R. Ochoukov, and D. G. Whyte, *Plasma Phys. Control. Fusion* **55**, 085001 (2013).
- ²¹ H. Kohno, J. R. Myra, and D. A. D’Ippolito, *Phys. Plasmas* **20**, 082514 (2013).
- ²² D. A. D’Ippolito and J. R. Myra, *Phys. Plasmas* **13**, 102508 (2006).
- ²³ E.F. Jaeger, L.A. Berry, J.S. Tolliver, D.B. Batchelor, *Phys. Plasmas* **2**, 2597 (1995).
- ²⁴ L. Colas, J. Jacquot, S. Heuraux, E. Faudot, K. Crombé, V. Korytsya, J. Hillairet, and M. Goniche, *Phys. Plasmas* **19**, 092505 (2012).
- ²⁵ M.A Lieberman, *IEEE Transactions on Plasma Science* **16**, 638 (1988).
- ²⁶ J. R. Myra and D. A. D’Ippolito, *Phys. Plasmas* **22**, 062507 (2015).
- ²⁷ M. A. Sobolewski, *Phys. Rev. E* **62**, 8540 (2000); and refs. therein.
- ²⁸ J. R. Myra and H. Kohno, “An Improved RF-Sheath Boundary Condition and Implications for ICRF Modeling,” 26th IAEA Fusion Energy Conference, Kyoto, Japan, 17-22 October 2016, IAEA-CN-234/TH-P4-31.
- ²⁹ U. Daybelge and B. Bein, *Phys. Fluids* **24**, 1190 (1981).
- ³⁰ R. Chodura, *Phys. Fluids* **25**, 1628 (1982).
- ³¹ K.-U. Riemann, *Physics of Plasmas* **1**, 552 (1994).
- ³² J. P. Gunn, *Physics of Plasmas* **4**, 4435 (1997); and refs. therein.
- ³³ R. Perkins, J.-W. Ahn, R. E. Bell, N. Bertelli, A. Diallo, S. P. Gerhardt, T. K. Gray, M. A. Jaworski, J. C. Hosea, G. J. Kramer, B. LeBlanc, R. Maingi, A. McLean, A. L. Roquemore, S. A. Sabbagh, T. Gary, and J. R. Wilson, “Large RF Field Amplitudes in the SOL and Far-Field RF Sheaths: A Proposed Mechanism for the Anomalous Loss of RF Power to the SOL of NSTX,” 26th IAEA Fusion Energy Conference, Kyoto, Japan, 17-22 October 2016, IAEA-CN-234/EX/P4-42.
- ³⁴ R. V. Nieuwenhove and G. V. Oost, *Plasma Phys. Control. Fusion* **34**, 525 (1992).
- ³⁵ E. Ahedo, *Phys. Plasmas* **6**, 4200 (1999).
- ³⁶ H. Kohno and J. R. Myra, manuscript submitted to *Comp. Phys. Comm.* (2017).
- ³⁷ F. W. Perkins, *Nucl. Fusion* **29**, 583 (1989).
- ³⁸ J. Moritz, E. Faudot, S. Devaux, and S. Heuraux, *Phys. Plasmas* **23**, 062509 (2016).
- ³⁹ D.L. Holland, B.D. Fried and G.J. Morales, *Phys. Fluids B* **5**, 1723 (1993).
- ⁴⁰ S. E. Parker X. Q. Xu, A. J. Lichtenberg and C. K. Birdsall, *Phys. Rev. A* **45**, 3949 (1992).
- ⁴¹ R. H. Cohen and D. Ryutov, *Phys. Plasmas* **6**, 1995 (1999).
- ⁴² D. D. Ryutov, *Contrib. Plasma Phys.* **36**, 207 (1996).

⁴³ H. Kohno, J. R. Myra, and D. A. D'Ippolito, *Phys. Plasmas* **22**, 072504 (2015); *ibid Phys. Plasmas* **23**, 089901 (2016).